RSC Advances

PAPER

View Article Online
View Journal | View Issue

Cite this: *RSC Adv.*, 2024, **14**, 40247

Trace amount of taurine leveling agent for stable Zn anode†

Xin Zhang,[a] Kai Zheng,[c] Dingyi Hu,[c] Si Liu *[b] and Zhifeng Lin*[b]

Aqueous zinc-ion batteries are highly praised for their cost-effectiveness, environmental friendliness, and high safety, making them an ideal choice for next-generation energy storage systems. However, the practical application of Zn metal anodes is constrained by well-known challenges such as dendrite growth and significant interfacial side reactions. This study introduces a trace amount of taurine (TAU) as a leveling additive into the electrolyte to optimize the microstructure of the electrolyte and the anode interface chemistry. On one hand, the preferential adsorption of TAU on the Zn surface promotes the *in situ* formation of a stable, protective molecular interfacial layer on the anode, which helps to refine the deposited grains and guide the uniform deposition of Zn^{2+}. On the other hand, the introduction of TAU can regulate the hydrogen bond structure in the electrolyte, reduce the activity of water, thereby significantly inhibiting the occurrence of side reactions such as hydrogen evolution. Consequently, the Zn//Zn symmetric cell system demonstrates an extended cycle life of over 1150 cycles at a current density of 1 mA cm^{-2} and maintains stable cycling performance for over 600 cycles at 10 mA cm^{-2}. Moreover, the Zn//Cu asymmetric cell system achieves over 1400 cycles of reversible deposition/dissolution at a current density of 1 mA cm^{-2}, with a coulombic efficiency of 99.4%. The incorporation of TAU further enhances the cycle stability of the Zn//MnO_2 full cell. These innovative achievements have laid a solid foundation for the broader industrial adoption of aqueous zinc-ion batteries.

Received 21st September 2024
Accepted 12th December 2024

DOI: 10.1039/d4ra06825d

rsc.li/rsc-advances

Introduction

In light of the progressive exhaustion of conventional fossil energy reserves, renewable energy sources such as solar and wind power are poised to emerge as integral components of the future energy portfolio for society.[1–3] The efficient storage of these intermittent renewable energy sources constitutes a pressing and pivotal challenge. Secondary battery energy storage systems that are both efficient and safe confer indispensable benefits in the optimization of energy supply infrastructures and in augmenting the efficiency of energy storage, conversion, and utilization, thereby assuming a central role in both academic research and industrial development.[4–6] Rechargeable aqueous zinc-ion batteries (AZIBs) are regarded as among the most promising candidates for subsequent-generation energy storage systems, attributable to their high safety profile, low cost, eco-friendliness, and adequate energy density.[7–9] Nevertheless, AZIBs confront challenges such as reduced coulombic efficiency and a limited cycle life, predominantly attributable to hydrogen evolution corrosion and dendrite formation, which substantially impede their deployment on a large scale.[10–12]

Electrolyte engineering, a straightforward and pragmatic approach, has been demonstrated to effectively tailor the solvation structure and the interface between the electrolyte and the anode.[13] The scholarly literature documents a variety of additives, including chelating ligands, organic solvents, polymers, metal salts, and quaternary ammonium salts, which have been shown to potently mitigate hydrogen evolution side reactions and control the deposition of zinc, thereby augmenting electrochemical performance.[14] Nonetheless, the reported concentrations of these additives in electrolytic solutions remain comparatively elevated, with a minimum of 1 g L^{-1}.[15,16] For instance, Zhang *et al.* introduced organic dimethylcarbonate 560 g L^{-1} DMC additive to form the 2 mol kg^{-1} $Zn(OTf)_2$ + 4H_2O + 1DMC (molar ratio) electrolytes, which successfully prolonged the lifetime of Zn//Zn half-cell to 1000 h at 1 mA cm^{-2} with 0.5 mA h cm^{-2}.[17] Wang *et al.* reported diethyl ether (142.3 g L^{-1}) as the additive of electrolyte, which can inhibit further deposition of zinc ions on the tip surface and resulted in stable operation for 250 h at current density of 0.2

[a]*Fujian Power Transmission and Transformation Engineering Co., Ltd, Fuzhou 350013, China*

[b]*Guangdong-Hong Kong-Macao Joint Laboratory for Intelligent Micro-Nano Optoelectronic Technology, School of Physics and Optoelectronic Engineering, School of Environmental and Chemical Engineering, Foshan University, Foshan 528000, China. E-mail: lius9@fosu.edu.cn; zhifenglin@fosu.edu.cn*

[c]*MOE Key Laboratory of Bioinorganic and Synthetic Chemistry, School of Chemistry, GBRCE for Functional Molecular Engineering, IGCME, Sun Yat-Sen University, Guangzhou 510275, China*

† Electronic supplementary information (ESI) available. See DOI: https://doi.org/10.1039/d4ra06825d

mA cm^{-2} with 0.5 mA h cm^{-2}.[18] Cao *et al.* introduced erythritol (6.1 g L^{-1}) as the functional additive for alters the coordination sphere of Zn^{2+} and modifies the local molecular architecture of the electrolyte. This modification serves to diminish the reactivity of water molecules, thereby efficaciously suppressing dendrite formation and deleterious ancillary reactions on the zinc powder anode surfaces, which successfully prolonged the lifetime of Zn//Zn half-cell to 850 h at 0.288 mA cm^{-2} with 0.144 mA h cm^{-2}.[19]

This study proposes a novel strategy for stabilizing the Zn anode in electrolytes by selecting levelers based on the molecular highest occupied molecular orbital (HOMO) energy levels. By adding an extremely low concentration of taurine (TAU) as an electrolyte additive (0.5 g L^{-1}), the stable and reversible deposition/dissolution of the Zn metal anode has been successfully achieved, providing key progress in the development of high-performance aqueous zinc-ion batteries. The study comprehensively employs *in situ* optical microscopy observations, density functional theory (DFT) calculations, and electrochemical experiments to delve into the underlying mechanism. The results indicate that TAU, due to its high HOMO energy level, exhibits significant adsorption capabilities, effectively adsorbing onto the Zn surface and regulating the nucleation and diffusion processes of interfacial Zn^{2+}, thereby achieving grain refinement and effectively inhibiting the growth of Zn dendrites. Concurrently, TAU can modulate the hydrogen bond network of the electrolyte, thereby effectively inhibiting hydrogen evolution side reactions. Based on this, the electrolyte system developed in this study has demonstrated outstanding stability, with the achieving over 1100 cycles of long-term cycle stability at a current density of 1 mA cm^{-2} and a capacity of 0.5 mA h cm^{-2} and over 240 cycles at 10 mA cm^{-2} and 2 mA h cm^{-2}, as well as high reversibility, as evidenced by an average coulombic efficiency of 99.4% for the Zn//Cu asymmetric cell. The Zn–Mn full cell fabricated in this study cycled more than 1000 times, exhibiting a capacity retention rate of approximately 73.8%. This research offers a directional framework for investigating cost-effective electrolyte additive engineering strategies aimed at achieving reversible and stable Zn anodes in high-performance Zn-based energy storage devices.

Results and discussion

Raman spectroscopy was used to investigate the microscopic structure of the electrolyte. As shown in Fig. S1,† the peaks at 3215.0 cm^{-1} and 3427.0 cm^{-1} correspond to symmetric and asymmetric vibrations, respectively, which may indicate different hydrogen-bonding environments within water clusters. After the addition of TAU as an electrolyte additive, these two broad bands undergo a significant blue shift, indicating that the introduction of TAU has altered the hydrogen-bonding environment in water.[20,21] Moreover, calculations based on molecular frontier orbital theory reveal that the HOMO energy level (E_{HOMO}) of the TAU molecule is −7.21 eV, in contrast to −8.35 eV for water molecules (Fig. 1a), implying that TAU exhibits a greater propensity to donate electrons and is thus more likely to adsorb onto the Zn surface by donating electrons

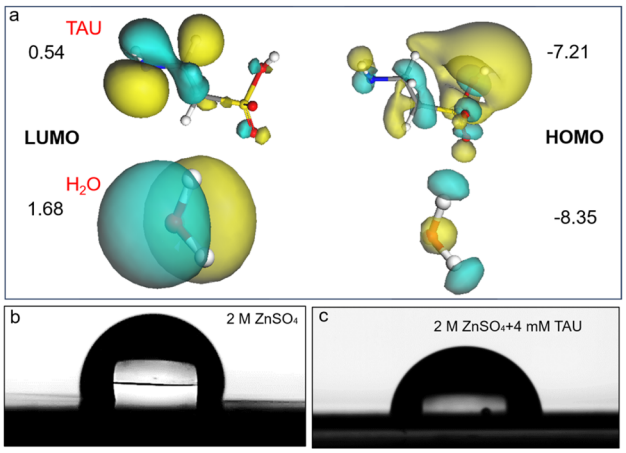

Fig. 1 (a) Energy levels of the highest occupied molecular orbital (HOMO) and the lowest unoccupied molecular orbital (LUMO) for TAU and H_2O; (b) contact angle of $ZnSO_4$ electrolyte on the surface of the Zn anode; (c) contact angle of $ZnSO_4$ electrolyte containing 4 mM TAU on the surface of the Zn anode.

to the vacant d-orbitals of the metal. Additionally, the wettability of the electrolyte on the Zn surface can influence the Zn^{2+} flux at the surface of the Zn anode to a certain degree.[22] Enhanced wettability promotes more uniform contact between Zn^{2+} ions and the Zn anode surface, thereby facilitating uniform nucleation of Zn. Water contact angle measurements demonstrate that the contact angle for a 2 M $ZnSO_4$ aqueous electrolyte is 94.9°, whereas the incorporation of TAU results in a reduced contact angle of 82.8° (Fig. 1c). This reduction is attributed to the effective adsorption of TAU on Zn, which diminishes the interfacial free energy between Zn and the electrolyte, thereby guiding the uniformization of Zn^{2+} flux.[23]

The impact of the TAU additive on the Zn electrodeposition process was visualized and documented through an *in situ* optical microscopy setup, focusing on a commercial Zn plate. As depicted in Fig. 2a–j, without the TAU additive, the deposition layer on the Zn surface was observed to be uneven, with pronounced protrusions emerging after 5 minutes of electrodeposition at a current density of 10 mA cm^{-2} (Fig. 2b). These

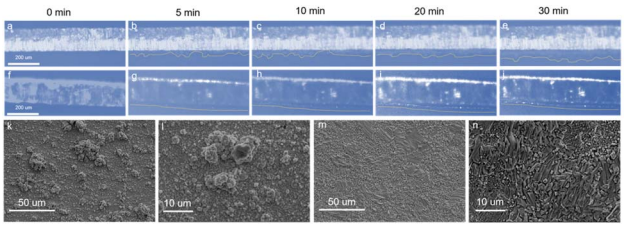

Fig. 2 *In situ* optical microscopy real-time recordings of the Zn deposition process on the Zn anode. (a)–(e) Deposition process in $ZnSO_4$ electrolyte; (f)–(j) deposition process in $ZnSO_4$ electrolyte supplemented with 4 mM TAU; (k) and (l) SEM image of the Zn surface after 0.5 h of electrodeposition at a current density of 10 mA cm^{-2} in $ZnSO_4$ electrolyte; (m) and (n) SEM image of the Zn surface after 0.5 h of electrodeposition at a current density of 10 mA cm^{-2} in $ZnSO_4$ electrolyte containing 4 mM TAU.

protrusions displayed touch-off and growth behaviors over time, a phenomenon known as the "tip effect" (Fig. 2e). In contrast, the addition of TAU led to a uniform Zn deposition process, effectively mitigating the formation of protrusions (Fig. 2f–j). Consequently, TAU significantly contributed to the attainment of a uniform and smooth Zn deposition (Fig. 2j). Furthermore, scanning electron microscopy (SEM) analysis revealed the micro morphology of the Zn surface following 0.5 h of electrodeposition at a current density of 10 mA cm^{-2}. Without TAU, the Zn coating displayed uneven growth with protrusions (Fig. 2k and l), whereas with TAU, the size of the Zn dendrite during the deposition process was significantly refined, and the resulting deposition layer exhibited a uniform and dense structural characteristic (Fig. 2m and n). This SEM test result is consistent with the observation results of the *in situ* optical microscope, confirming the results of the *in situ* optical microscope test.

To assess the corrosion resistance of the Zn electrode in the presence of TAU, Tafel polarization tests were conducted. As illustrated in Fig. 3a, the self-corrosion current densities were ascertained by extrapolating the linear portion of the polarization curves, with the potential at the minimum current density being designated as the corrosion potential (E_{corr}). The Zn electrode immersed in pure 2 M $ZnSO_4$ displayed an E_{corr} of −0.975 V, whereas in the electrolyte augmented with TAU, the E_{corr} was slightly higher at −0.981 V, suggesting a negligible disparity. The self-corrosion current density (J_{corr}) of the Zn electrode in the pure 2 M $ZnSO_4$ electrolyte was measured at 3.30 mA cm^{-2}, whereas in the TAU-enriched electrolyte, it was reduced to 1.75 mA cm^{-2}. To further examine the anti-corrosion properties for different electrolyte, the Zn foils were immersed into electrolytes with and without 4 mM TAU for 5 days. X-ray Diffraction (XRD) patterns results revealed that the diffraction peak of basic zinc sulfate (Fig. S2†) pentahydrate ($Zn_4SO_4(OH)_6 \cdot 5H_2O$ PDF# 39-0688) appeared for the Zn in the normal electrolyte,[24] indicating that there was a certain amount of alkali pentahydrate formed on the surface of Zn sulfate. In contrast, in the TAU electrolyte, there was no appearance of the diffraction peak for basic Zn sulfate pentahydrate, indicating that TAU can effectively inhibit the corrosion of Zn. These findings indicate that TAU effectively mitigates the self-corrosion rate of the Zn electrode within the electrolyte.[25] The linear sweep voltammetry (LSV) curves (Fig. 3b) demonstrated that at a current density of 1 mA cm^{-2}, the hydrogen evolution potential was −1.39 V in the 1 M Na_2SO_4 + 0 mM TAU electrolyte, and −1.48 V in the 1 M Na_2SO_4 + 4 mM TAU electrolyte. This discrepancy is likely attributed to TAU adsorbing onto the Zn electrode surface and suppressing side reactions.[26]

To elucidate the Zn deposition behavior within diverse electrolytes, chronopotentiometric studies were conducted. At an overpotential of −0.15 V, the current–time profile delineated nucleation and surface alterations. Over a 300 s interval, in a pristine $ZnSO_4$ electrolyte, the current progressively escalated, implying a two-dimensional (2D) diffusion mechanism and the formation of uneven dendrites on the Zn anode surface (Fig. 4a). Within the 2D diffusion phase, adsorbed Zn^{2+} ions diffuse laterally along the electrode surface, aggregate at the tips, and subsequently morph into Zn dendrites. Conversely, in a $ZnSO_4$ electrolyte supplemented with TAU, the zinc electrode displayed a stable current density following a transient 2D diffusion phase, indicating a steady 3D diffusion process subsequent to nucleation. The 3D diffusion suggests that adsorbed Zn^{2+} ions are locally reduced to Zn, with 2D surface diffusion being constrained. This behavior can be ascribed to the inhibitory effect of adsorbed TAU on Zn^{2+} diffusion.[27] Concurrently, the cyclic voltammetry (CV) curve of a pure 2 M $ZnSO_4$ electrolyte exhibited a pronounced oxidation peak, whereas the oxidation peak attenuated upon the incorporation of TAU, indicative of enhanced reversibility in the deposition and dissolution of Zn (Fig. 4b).[28] Coulombic efficiency is pivotal for the stability of reversible Zn deposition/dissolution processes. Reversible deposition/dissolution tests were carried out using Zn//Cu asymmetric cells. Fig. 4c juxtaposes the cycle stability of Zn//Cu asymmetric cells in electrolytes with and without 4 mM TAU. In the pristine $ZnSO_4$ electrolyte, at a current density of 1 mA cm^{-2} and a surface capacity of 0.5 mA h cm^{-2}, the Zn//Cu asymmetric cell exhibited a rapid decline after approximately 100 deposition/dissolution cycles, attributed to localized short-circuiting resulting from Zn dendrite growth during cycling. At the 100th cycle, the battery displayed fluctuating voltage profiles and short-circuiting, with

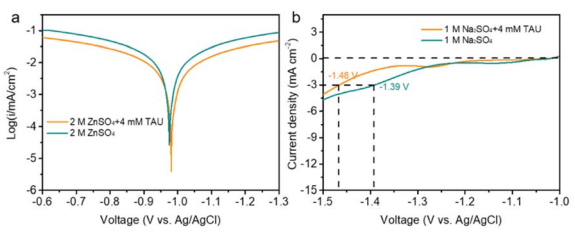

Fig. 3 (a) Tafel plots for the Zn anode in $ZnSO_4$ and $ZnSO_4$ + 4 mM TAU electrolytes; (b) linear sweep voltammetry curves for the anode in Na_2SO_4 and Na_2SO_4 + 4 mM TAU electrolytes.

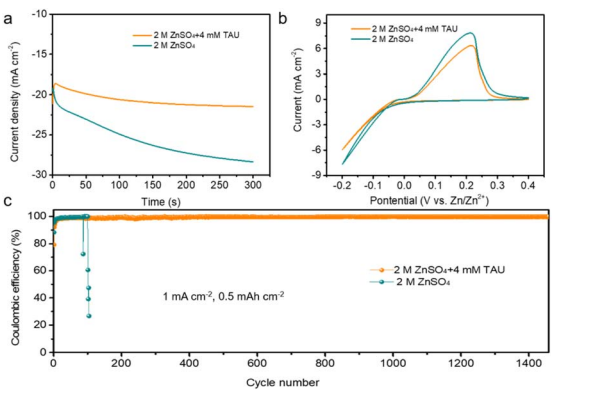

Fig. 4 (a) Comparison of chronamperometric tests conducted in $ZnSO_4$ and $ZnSO_4$ + 4 mM TAU electrolytes; (b) cyclic voltammetry curves for the electrolytes $ZnSO_4$ and $ZnSO_4$ + 4 mM TAU; (c) coulombic efficiency of the Zn//Cu asymmetric cells in $ZnSO_4$ and $ZnSO_4$ + 4 mM TAU electrolytes (1 mA cm^{-2}, 0.5 mA h cm^{-2}).

an average coulombic efficiency of 96.7%. Notably, the initial-cycle coulombic efficiency of the Zn//Cu asymmetric cell in a 4 mM TAU-enriched $ZnSO_4$ electrolyte is 79.2%. With the progression of cycles, the coulombic efficiency improves. By the 50th cycle, the efficiency surpasses 99%. Furthermore, the Zn//Cu asymmetric cell demonstrates exceptional stability, lasting for 1459 cycles, with an average coulombic efficiency of 99.4%. This performance exceeds the levels previously reported in the studies.[28–32] Meanwhile, Fig. S3† shows the voltage distribution diagrams of Zn//Cu asymmetric cells over different cycles. In the electrolyte with the TAU additive, the voltage distribution curves of the Zn//Cu asymmetric cell remain unchanged during the 1st–5th cycles, the 600th–800th cycles, and the 1400th–1460th cycles. In contrast, in the $ZnSO_4$ electrolyte, a short circuit occurs at the 100th cycle. Furthermore, at a higher current density of 10 mA cm^{-2} and a higher areal capacity of 2 mA h cm^{-2}, the Zn//Cu asymmetric cell with the TAU additive electrolyte also cycles stably for more than 120 cycles (Fig. S4a†). In the $ZnSO_4$ electrolyte, after 75 cycles, the polarization increases (Fig. S4b†), and the cell fails after 90 cycles. These results further indicate that TAU can effectively improve the stability of the cell.

In order to study the plating/stripping kinetics of Zn anodes in different electrolytes, cyclic voltammetry (CV) tests were conducted. Fig. S5a† shows the CV cycle curves of Zn//Zn symmetric cells in different electrolytes at 0.1 mV s^{-1}. Compared to the normal electrolyte, the Zn anode exhibits a larger peak area and a slightly reduced current due to adsorption, which is related to the faster plating/stripping kinetics caused by the addition of TAU additive.[31] Moreover, the electrochemical kinetics of Zn^{2+} at the electrode interface were further explored through electrochemical impedance spectroscopy (EIS) measurements. Fig. S5b† shows the Nyquist plots of Zn//Zn symmetric cells in different electrolytes, where the semicircles in high and medium frequencies correspond to the charge transfer resistance. The introduction of the TAU additive significantly reduces the charge transfer resistance of the Zn//Zn symmetric cell, indicating its superior charge transfer performance.[14]

To corroborate the influence of TAU on the performance of the Zn anode, the electrochemical behavior of Zn//Zn symmetric cells was scrutinized in both a pure $ZnSO_4$ electrolyte and an electrolyte fortified with TAU. As illustrated in Fig. 5a, under the 1 mA cm^{-2} current density and 0.5 mA h cm^{-2} surface capacity, the Zn//Zn symmetric cell employing TAU as an additive exhibited sustained cycling for over 1150 cycles, substantially exceeding the duration of 200 cycles for the control without TAU, also exceeds the levels reported in previous studies.[33,34] At an elevated current density of 10 mA cm^{-2} and surface capacity of 2 mA h cm^{-2}, the TAU-containing Zn//Zn symmetric cell sustained stable cycling for over 600 cycles, whereas the cell relying on the pure $ZnSO_4$ electrolyte deteriorated after only 250 cycles, underscoring the effectiveness of TAU in bolstering the stability of Zn//Zn symmetric cells (Fig. 5b). The rate performance of symmetric cell is shown on Fig. S5,† where the current density gradually increased from 1 mA cm^{-2} to 10 mA cm^{-2}. Obviously, the hysteresis voltage of the Zn//Zn symmetric cell

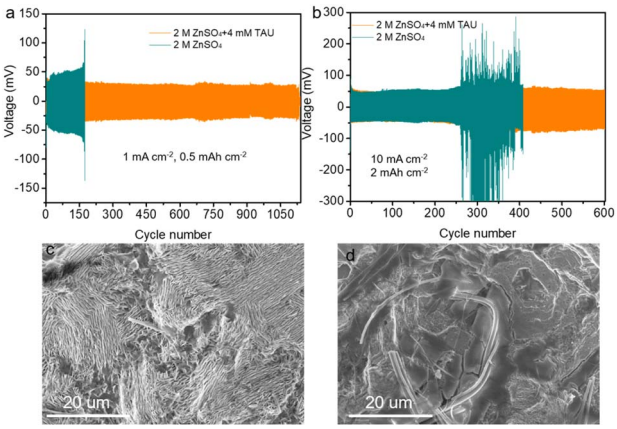

Fig. 5 (a) Cycling curves of the Zn//Zn symmetric cell in $ZnSO_4$ and $ZnSO_4$ + 4 mM TAU electrolytes (at 1 mA cm^{-2} and 0.5 mA h cm^{-2}); (b) cycling curves of the Zn//Zn symmetric cell in $ZnSO_4$ and $ZnSO_4$ + 4 mM TAU electrolytes (at 10 mA cm^{-2} and 2 mA h cm^{-2}); (c) SEM image of the Zn//Zn symmetric cell after 100 cycles in $ZnSO_4$ + 4 mM TAU electrolyte (at 1 mA cm^{-2} and 0.5 mA h cm^{-2}); (d) SEM image of the Zn//Zn symmetric cell after 100 cycles in $ZnSO_4$ electrolyte (at 1 mA cm^{-2} and 0.5 mA h cm^{-2}).

with TAU-added electrolyte is smaller than that of the Zn//Zn symmetric cell with normal electrolyte due to TAU exhibits a greater propensity to donate electrons and is thus more likely to adsorb onto the Zn surface by donating electrons to the vacant d-orbitals of the metal. In addition, as the current density increases, the Zn//Zn symmetric cell with normal electrolyte rapidly polarization increases and fails at 10.0 mA cm^{-2}. Oppositely, the Zn//Zn symmetric cell with the TAU-added electrolyte maintained the stable deposition/stripping process and remained functional even after the current density returned to 1 mA cm^{-2}. The Zn//Zn symmetric cell could still run steadily even at an ultrahigh current density of 20 mA cm^{-2} and areal capacity of 5 mA h cm^{-2} (Fig. S7†). The Zn//Zn symmetric cell with the TAU electrolyte could sustain steadily plating/stripping processes over 300 cycles, whereas the Zn//Zn symmetric cell in the normal electrolyte undergoes severe polarization after 14 cycles, which signifies that TAU additive can fulfill the demands of actual devices. Furthermore, following 100 stripping/plating cycles at 1 mA cm^{-2}, SEM images depicted that the morphology of the Zn anode with TAU as an additive was characterized by a flat and protrusion-free surface (Fig. 5c), in stark contrast to the original electrolyte electrode, which was encrusted with a multitude of vertical protrusions and voids (Fig. 5d), thereby indicating that TAU effectively curtails dendrite formation. XPS analysis of the Zn foil surface after symmetric cell cycling to determine the adsorption during cycling. To confirm the mechanism of action of TAU, based on the Zn anode surface after symmetric cell cycling in the TAU electrolyte using XPS and Energy Dispersive Spectrometer (EDS) mapping, the Zn, O, N, C and S signals can be observed (Fig. S8a and b†). The C 1s core-level XPS spectra is displayed in Fig. S8c.† The C 1s spectra of the non-sputtered anode exhibited peaks at 288.2, 286.2, and 284.8 eV, attributable to C–S, C–O/C–N, and C–C/C–H.[13] The S 2p and Zn 2p core-level XPS spectrum remained

almost unchanged, demonstrating that TAU is not subject to decomposition (Fig. S8d and S9†).[6] As demonstrated in Fig. S9,† EDS mapping images prove that the Zn, O, N, C and S elements are uniformly distributed in Zn anode surface. These analysis results indicate that TAU can be adsorbed on the Zn anode surface.

To delineate the impact of TAU additive on the full battery cycling performance, we synthesized pure α-MnO_2@CNT nanowires through hydrothermal processing. Initial characterization of the α-MnO_2@CNT positive electrode was performed using SEM, as depicted in Fig. S2a,† which revealed the formation of MnO_2 nanowires in a homogeneously dispersed matrix with carbon nanotubes (CNTs). The X-ray diffraction (XRD) pattern in Fig. S2b† confirmed the formation of α-phase MnO_2 (PDF No. 44-0141) without any discernible impurity peaks.[35] To ascertain the carbon content within the MnO_2@CNT composite, thermal gravimetric analysis (TGA) was conducted, which yielded a carbon content of 24.3% for α-MnO_2@CNT (Fig. S2c†). As depicted in Fig. 6, the Zn//MnO_2 full battery utilizing TAU-containing electrolyte exhibited a superior capacity retention rate of 73.8% after 1000 cycles. In stark contrast, the Zn//MnO_2 full battery employing the original electrolyte retained only 24.4% of its initial capacity. The gravimetric charge discharge curve (GCD) of the Zn//MnO_2 full cell using different electrolytes are shown in Fig. S11a and b.† The full cell with TAU electrolyte has significantly higher capacity and more stable discharge plateau at the 100th cycle. These findings underscore the efficacy of the electrolyte additive in bolstering the cycling performance of full batteries.

Based on the above experimental results and theoretical calculations, we propose a possible mechanism by which the TAU additive inhibits the formation of Zn dendrites in normal electrolyte systems. As shown in the schematic diagram in Fig. 7, during the nucleation stage, in order to minimize surface energy and the exposed area of the electrode, Zn^{2+} adsorbed on the electrode surface tend to diffuse laterally along the surface and aggregate, forming a large number of dispersed crystal nuclei. In the subsequent deposition process, continuous lateral diffusion and the tip effect cause the crystal nuclei to grow rapidly, forming Zn dendrites, which leads to a vicious cycle resulting in the formation of a large number of Zn dendrites on the electrode surface. However, when an appropriate concentration of TAU additive is present in the electrolyte, TAU not only participates in the solvation of Zn^{2+} but also adsorbs on the surface of the Zn anode, regulating the lateral

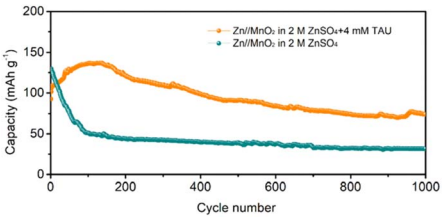

Fig. 6 Comparison of cycling performance for the Zn//MnO_2 full cell in different electrolytes.

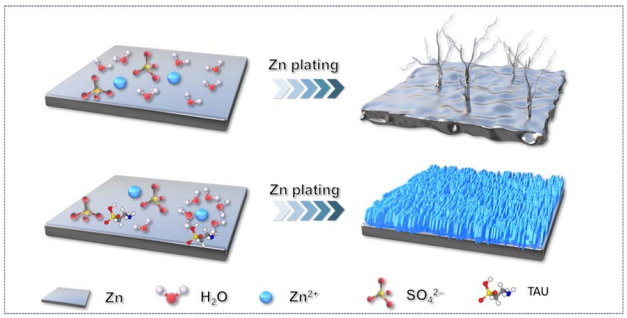

Fig. 7 Schematic diagram of the deposition behavior of Zn^{2+} in electrolytes without and with additives.

diffusion and aggregation of Zn^{2+} during the nucleation stage, and promoting the formation of uniform crystal nuclei. In the subsequent deposition process, the tip effect causes TAU to preferentially aggregate at the tips or protrusions of the electrode surface, forming an effective zinc-repelling barrier layer that effectively inhibits the adsorption and deposition of Zn^{2+} in these areas, thereby promoting the uniform adsorption and deposition of Zn^{2+} on the electrode surface.

Conclusion

In summary, this study has successfully developed an efficient, non-toxic, and cost-effective TAU electrolyte additive, which can simultaneously optimize the adsorption behavior on the surface of the Zn anode and the hydrogen bond network in the electrolyte, thereby effectively promoting the formation of a dendrite-free and stable Zn anode. Experimental results have confirmed the leveling effect of the TAU additive, which not only effectively refined the deposited grains and inhibited the growth of Zn dendrites but also significantly suppressed the occurrence of side reactions such as HER by altering the hydrogen bond network in the electrolyte, thereby promoting the uniform deposition of Zn^{2+}. In the tests of Zn//Zn symmetric cells, the electrolyte containing TAU exhibited stable cycling performance for over 1150 cycles at a current density of 1 mA cm^{-2}. Moreover, under a current density of 10 mA cm^{-2} and a cycle capacity of 2 mA h cm^{-2}, the system maintained stable cycling for over 600 cycles. Notably, the Zn//Cu asymmetric cell in a 4 mM TAU-enriched $ZnSO_4$ electrolyte achieved an average coulombic efficiency of 99.4% and maintained stability for 1459 cycles. Surprisingly, the Zn//MnO_2 full battery prepared using this electrolyte retained a high capacity retention rate of 73.8% after 1000 cycles. Notably, these electrochemical performance metrics significantly surpass those of the control group using the original electrolyte, further verifying the remarkable effect of the TAU additive in enhancing the performance of the zinc anode. The results of this study emphasize the importance of incorporating TAU, an economical and environmentally friendly additive, into the electrolyte, providing a simple and effective strategy for the development of highly reversible Zn anodes and stable aqueous zinc-ion batteries.

Experimental section

Preparation of Zn anode

The preparation of the Zn anode involved initially degreasing commercial Zn flakes (purity: 99.999%, supplier: Alfa Aesar) at 60 °C for 10 minutes in a 150 mL mixed aqueous solution. This solution comprised 4.5 g of Na_2CO_3 (purity: 99.5%, supplier: Aladdin), 1.5 g of $Na_2SiO_3 \cdot 5H_2O$ (analytical reagent, supplier: Aladdin), 3.0 g of $Na_3PO_4 \cdot 12H_2O$ (purity: 99%, supplier: Aladdin), and 0.75 mL of OP-10 (analytical reagent, supplier: Kermel). Subsequently, the degreased Zn flakes were sonicated in absolute ethanol and acetone for 30 minutes.

Preparation of α-MnO_2/CNT

3.4 g of manganese(II) acetate tetrahydrate (analytical reagent, supplier: Aladdin) and 0.3 g of carboxyl-functionalized carbon nanotubes were added to 75 mL of distilled water. The resulting mixture was then slowly added dropwise to 80 mL of an aqueous solution containing 1.45 g of potassium permanganate (analytical reagent, supplier: Guangshi). The combined solution was stirred for 30 minutes before being placed in an 80 °C incubator and heated for 6 hours. After this period, the resultant dark brown precipitate was washed several times with deionized water and dried in an 80 °C oven until all water had evaporated, yielding the α-MnO_2/CNT nanocomposites.

Characterization

The surface morphologies and microstructures of all samples were examined using a field-emission scanning electron microscope (SEM, Thermo Fisher Quatro S) with acceleration voltage 15 kV, and utilizing secondary electron or backscattered electron signals to perform surface topography analysis on the microstructures of Zn electrode. Laser Raman spectroscopy (Raman, inVia) with a 532 nm wavelength was employed to analyze the functional groups or chemical bonds present. Carbon content was determined by thermogravimetric analysis (STA449F5). X-ray diffraction (XRD) analysis was conducted on a Rigaku D-MAX 2200 VPC instrument using Cu Kα radiation. The real-time observation of zinc deposition was recorded with a Leica DM2700P optical microscope.

Electrochemical measurements

Tafel curves were measured on an electrochemical workstation (CHI760E) with zinc plates as the working electrodes, a graphite rod as the counter electrode, and an Ag/AgCl electrode as the reference electrode, using 2 M $ZnSO_4$ (purity: 99.5%, supplier: Aladdin) as the electrolyte. Linear polarization curves were recorded by scanning the voltage from −1.3 to −0.6 V at a rate of 10 mV s^{-1}. Linear sweep voltammetry (LSV) was performed at 5 mV s^{-1} on the same electrochemical workstation using zinc plates as the working electrode, a graphite rod as the counter electrode, an Ag/AgCl electrode as the reference electrode, and 1 M Na_2SO_4 with or without TAU (analytical reagent, purity: 99.5%, supplier: Aladdin) as the electrolyte. Chronoamperometry was conducted on the electrochemical workstation with zinc plates serving as both the working and counter electrodes, an Ag/AgCl electrode as the reference electrode, and 2 M $ZnSO_4$ as the electrolyte. Chronoamperometry curves were recorded by scanning the voltage at −0.15 V relative to the open-circuit potential.

DFT calculation method

All the calculations were performed by density functional theory (DFT) using the Materials Studio 5.5 package. The structures were optimized and the properties were calculated by the DMol3 module. The hybrid function B3LYP was employed. The convergence tolerance of energy, force and displacement convergence were set as 1×10^{-5} Ha, 2×10^{-3} Å and 5×10^{-3} Å, respectively. The core treatment was chosen as the effective core potential (ECP), and the electron treatment was performed by double numerical plus d-functions (DNP) basis set.

Data availability

The datasets generated and/or analysed during the current study are not publicly available, but are available from the corresponding author on reasonable request.

Conflicts of interest

The authors report no declarations of interest.

Acknowledgements

This work was received the financial support by the research Fund of Guangdong-Hong Kong-Macao Joint Laboratory for Intelligent Micro-Nano Optoelectronic Technology (No. 2020B1212030010).

Notes and references

1 Z. Yu, H. W. Kamran, A. Amin, B. Ahmed and S. Peng, Sustainable Synergy via Clean Energy Technologies and Efficiency Dynamics, *Renewable Sustainable Energy Rev.*, 2023, **187**, 113744.
2 Z. Zhu, T. Jiang, M. Ali, Y. Meng, Y. Jin, Y. Cui and W. Chen, Rechargeable Batteries for Grid Scale Energy Storage, *Chem. Rev.*, 2022, **122**, 16610–16751.
3 Z. Feng, Y. Feng, F. Fan, D. Deng, H. Dong, S. Liu, L. Kang, S. Jun, L. Wang, J. Zhu, L. Dai and Z. He, Functionalization Design of Zinc Anode for Advanced Aqueous Zinc-Ion Batteries, *SusMat*, 2024, **4**, e184.
4 M. Wang, Y. Meng, M. Sajid, Z. Xie, P. Tong, Z. Ma, K. Zhang, D. Shen, R. Luo, L. Song, L. Wu, X. Zheng, X. Li and W. Chen, Bidentate Coordination Structure Facilitates High-Voltage and High-Utilization Aqueous Zn-I(2) Batteries, *Angew Chem. Int. Ed. Engl.*, 2024, **63**, e202404784.
5 W. Hu, J. Ju, N. Deng, M. Liu, W. Liu, Y. Zhang, L. Fan, W. Kang and B. Cheng, Recent Progress in Tackling Zn Anode Challenges for Zn Ion Batteries, *J. Mater. Chem. A*, 2021, **9**, 25750–25772.

6 G. Duan, Y. Wang, B. Luo, L. Sun, S. Zheng, J. Huang and Z. Ye, Taurine-Mediated Dynamic Bridging Strategy for Highly Stable Zn Metal Anode, *Energy Storage Mater.*, 2023, **61**, 102882.
7 M. Liu, *et al.*, Nanoscale Ultrafine Zinc Metal Anodes for High Stability Aqueous Zinc Ion Batteries, *Nano Lett.*, 2023, **23**, 541–549.
8 Z. Xie, N. Chen, M. Zhang, M. Wang, X. Zheng, S. Liu, R. Lou, L. Song, Y. Meng, Z. Liu, Z. Li and W. Chen, Carbonate-Assisted Chaotropic Electrolyte for Zinc Ion Battery with Wide Temperature Operation, *ACS Energy Lett.*, 2024, **9**, 3380–3390.
9 Y. Shang and D. Kundu, A Path Forward for the Translational Development of Aqueous Zinc-Ion Batteries, *Joule*, 2023, **7**, 244–250.
10 L. Hong, X. Wu, L. Y. Wang, M. Zhong, P. Zhang, L. Jiang, W. Huang, Y. Wang, K. X. Wang and J. S. Chen, Highly Reversible Zinc Anode Enabled by a Cation-Exchange Coating with Zn-Ion Selective Channels, *ACS Nano*, 2022, **16**, 6906–6915.
11 Y. Meng, M. Wang, J. Wang, X. Huang, X. Zhou, M. Sajid, Z. Xie, R. Luo, Z. Zhu, Z. Zhang, N. Khan, Y. Wang, Z. Li and W. Chen, Robust Bilayer Solid Electrolyte Interphase for Zn Electrode with High Utilization and Efficiency, *Nat. Commun.*, 2024, **15**, 8431.
12 X. Zhou, T. Ruan, J. Xu, C. Li, S. Huang, J. Zhou, S. Lu, R. Song and R. Li, Host-Design Strategies of Zinc Anodes for Aqueous Zinc-Ion Batteries, *RSC Adv.*, 2024, **14**, 23023–23036.
13 Y. Xu, J. Qin, R. Liu, H. Feng, X. Wang, M. Li, M. Sun, W. Shi, W. Xiao, B. Su and Y. Cheng, Simultaneous Regulation on Coordination Environment and Interfacial Chemistry via Taurine for Stabilized Zn Metal Anode, *J. Energy Chem.*, 2023, **86**, 343–350.
14 K. Ouyang, S. Chen, W. Ling, M. Cui, Q. Ma, K. Zhang, P. Zhang and Y. Huang, Synergistic Modulation of in-Situ Hybrid Interface Construction and Ph Buffering Enabled Ultra-Stable Zinc Anode at High Current Density and Areal Capacity, *Angew Chem. Int. Ed. Engl.*, 2023, **62**, e202311988.
15 H. Dai, K. Xi, X. Liu, C. Lai and S. Zhang, Cationic Surfactant-Based Electrolyte Additives for Uniform Lithium Deposition via Lithiophobic Repulsion Mechanisms, *J. Am. Chem. Soc.*, 2018, **140**, 17515–17521.
16 A. Bayaguud, X. Luo, Y. Fu and C. Zhu, Cationic Surfactant-Type Electrolyte Additive Enables Three-Dimensional Dendrite-Free Zinc Anode for Stable Zinc-Ion Batteries, *ACS Energy Lett.*, 2020, **5**, 3012–3020.
17 Y. Dong, L. Miao, G. Ma, S. Di, Y. Wang, L. Wang, J. Xu and N. Zhang, Non-Concentrated Aqueous Electrolytes with Organic Solvent Additives for Stable Zinc Batteries, *Chem. Sci.*, 2021, **12**, 5843–5852.
18 W. Xu, K. Zhao, W. Huo, Y. Wang, G. Yao, X. Gu, H. Cheng, L. Mai, C. Hu and X. Wang, Diethyl Ether as Self-Healing Electrolyte Additive Enabled Long-Life Rechargeable Aqueous Zinc Ion Batteries, *Nano Energy*, 2019, **62**, 275–281.
19 H. Liu, P. Cao, Y. Chen, C. Chen, S. Fan, C. Li, H. Zhu, M. Wu and J. Yang, Stabilization of Flake Zn Powder Anodes via Designing Functional Additives in Electrolytes for Aqueous Zn Ion Batteries, *J. Energy Chem.*, 2024, **99**, 139–148.
20 H. Yang, Z. Chang, Y. Qiao, H. Deng, X. Mu, P. He and H. Zhou, Constructing a Super-Saturated Electrolyte Front Surface for Stable Rechargeable Aqueous Zinc Batteries, *Angew Chem. Int. Ed. Engl.*, 2020, **59**, 9377–9381.
21 H. Ren, S. Li, B. Wang, Y. Zhang, T. Wang, Q. Lv, X. Zhang, L. Wang, X. Han, F. Jin, C. Bao, P. Yan, N. Zhang, D. Wang, T. Cheng, H. Liu and S. Dou, Molecular-Crowding Effect Mimicking Cold-Resistant Plants to Stabilize the Zinc Anode with Wider Service Temperature Range, *Adv. Mater.*, 2023, **35**, e2208237.
22 W. Wang, G. Huang, Y. Wang, Z. Cao, L. Cavallo, M. N. Hedhili and H. N. Alshareef, Organic Acid Etching Strategy for Dendrite Suppression in Aqueous Zinc-Ion Batteries, *Adv. Energy Mater.*, 2022, **12**, 2102797.
23 G. Ma, L. Miao, Y. Dong, W. Yuan, X. Nie, S. Di, Y. Wang, L. Wang and N. Zhang, Reshaping the Electrolyte Structure and Interface Chemistry for Stable Aqueous Zinc Batteries, *Energy Storage Mater.*, 2022, **47**, 203–210.
24 R. Zhao, Y. Yang, G. Liu, R. Zhu, Z. Chen, Z. Gao, X. Chen and L. Qie, Redirected Zn Electrodeposition by an Anti-Corrosion Elastic Constraint for Highly Reversible Zn Anodes, *Adv. Funct. Mater.*, 2021, **31**, 2001867.
25 Y. Ai, *et al.*, Biomimetic Superstructured Interphase for Aqueous Zinc-Ion Batteries, *J. Am. Chem. Soc.*, 2024, **146**, 15496–15505.
26 C. Li, X. Zhang, G. Qu, S. Zhao, H. Qin, D. Li, N. Li, C. Wang and X. Xu, Highly Reversible Zn Metal Anode Securing by Functional Electrolyte Modulation, *Adv. Energy Mater.*, 2024, **14**, 2400872.
27 F. Zhao, J. Feng, H. Dong, R. Chen, T. Munshi, I. Scowen, S. Guan, Y. Miao, T. Liu, I. Parkin and G. He, Ultrathin Protection Layer via Rapid Sputtering Strategy for Stable Aqueous Zinc Ion Batteries, *Adv. Funct. Mater.*, 2024, 2409400.
28 J. Li, Z. Guo, J. Wu, Z. Zheng, Z. Yu, F. She, L. Lai, H. Li, Y. Chen and L. Wei, Dextran: A Multifunctional and Universal Electrolyte Additive for Aqueous Zn Ion Batteries, *Adv. Energy Mater.*, 2023, **13**, 2301743.
29 Q. Zhang, L. Deng, M. Li, X. Wang, R. Li, Z. Liu, C. Yang, X. Wang, W. Liu and Y. Yu, Regulation of Zinc Interface by Maltitol for Long-Life Dendrite-Free Aqueous Zinc Ion Batteries, *J. Electron. Mater.*, 2022, **51**, 4763–4771.
30 F. Tao, K. Feng, Y. Liu, J. Ren, Y. Xiong, C. Li and F. Ren, Suppressing Interfacial Side Reactions of Zinc Metal Anode via Isolation Effect toward High-Performance Aqueous Zinc-Ion Batteries, *Nano Res.*, 2023, **16**, 6789–6797.
31 S. Chen, D. Ji, Q. Chen, J. Ma, S. Hou and J. Zhang, Coordination Modulation of Hydrated Zinc Ions to Enhance Redox Reversibility of Zinc Batteries, *Nat. Commun.*, 2023, **14**, 3526.
32 Y. Liu, J. Hu, Q. Lu, M. Hantusch, H. Zhang, Z. Qu, H. Tang, H. Dong, O. Schmidt, R. Holze and M. Zhu, Highly Enhanced Reversibility of a Zn Anode by in-Situ Texturing, *Energy Storage Mater.*, 2022, **47**, 98–104.

33 B.-b. Sui, L. Sha, P.-f. Wang, Z. Gong, Y.-h. Zhang, Y.-h. Wu, L.-n. Zhao, J.-j. Tang and F.-n. Shi, In Situ Zinc Citrate on the Surface of Zn Anode Improves the Performance of Aqueous Zinc-Ion Batteries, *J. Energy Storage*, 2024, **82**, 110550.

34 X. Yu, T. Zhang, D. Yu, T. Tian, H. Niu, W. Yang and D. Sun, Stabilizing Zn Anodes via a Binder-Free MoS_2 Interface with Charge Regulation toward Stable Zinc-Ion Batteries, *Chem. Eng. Sci.*, 2024, **299**, 120523.

35 J. Xu, X. Hu, M. A. Alam, G. Muhammad, Y. Lv, M. Wang, C. Zhu and W. Xiong, Al-Doped α-MnO_2 Coated by Lignin for High-Performance Rechargeable Aqueous Zinc-Ion Batteries, *RSC Adv.*, 2021, **11**, 35280–35286.